Groundwater

Aquifer Imaging with Oscillatory Hydraulic Tomography: Application at the Field Scale

by Michael Cardiff[1,2], YaoQuan Zhou[1,3], Warren Barrash[4], and Peter K. Kitanidis[5]

Abstract

Modeling and laboratory experiments have demonstrated the ability of oscillatory hydraulic tomography (OHT) to characterize heterogeneity in aquifer hydraulic properties. In OHT, a location is stressed via periodic pumping/injection at a set frequency, and the resulting head signal is measured at a number of monitoring locations. The source of oscillations is repeatedly moved, allowing tomographic imaging of aquifer properties. Changing the period of oscillation also results in observations with additional information. In theory, OHT is comparable to other hydraulic tomography methods in that distributed pressure change measurements provide characterization information. In practice, OHT has several benefits including: (1) little to no water injected into or extracted from the aquifer; and (2) an observational signal at a set period that can be easily extracted in the presence of noise. We report the first field application of OHT, carried out at the Boise Hydrogeophysical Research Site (BHRS) using an oscillating signal generator with a very small cycling volume of <2 L, and a period range of 5 to 70 s. For these tests, signals were detected at distances of over 15 m. After processing to extract periodic signal properties, we perform tomography using a frequency-domain numerical model for groundwater flow. In comparing results against prior characterization results from the BHRS, we find moderate to strong positive correlations between K profiles estimated via different methods at multiple wells, with moderate overall correlation between estimated three-dimensional (3D) K volumes.

Introduction

Understanding subsurface heterogeneity in the sediment and rock properties that control fluid flow is fundamental to understanding processes including the transport and mixing of solutes in groundwater. The difficulty in effectively mapping this heterogeneity—especially in hydraulic conductivity (K)—represents a continual challenge for hydrogeology. Many technologies have been suggested to help map this variability, spanning hydrogeologic (pressure-based/tracer-based) and geophysical methods. Hydraulic tomography (HT) is one such technology, which has been suggested and tested as a method for aquifer characterization, since being first suggested almost 25 years ago (Gottlieb and Dietrich 1995). At its most basic level, HT represents any technology in which: (1) pressure/head change data from a set of sensors is recorded at multiple locations during a series of different pumping tests; and (2) the collected data is analyzed tomographically, that is, by fitting all data jointly within a heterogeneous (distributed parameter) numerical model. Relative to other characterization methods, a fundamental benefit of HT surveys is that multiple testing arrangements can be performed over a timeframe comparable to a single tracer test and—unlike geophysical methods—they are directly sensitive to the variability of hydraulic parameters between boreholes. Inversion of data from HT surveys provides an opportunity to constrain aquifer parameters beyond the vicinity of a wellbore. In terms of practical utility, several recent studies have examined the effectiveness of HT at the field scale (Berg and Illman 2014; Cardiff et al. 2012, 2013a; Hochstetler et al. 2016; Tiedeman and Barrash 2019). While promising characterization results have demonstrated the method's effectiveness, refinement of the technology to reduce time and financial costs associated with data collection, screening, processing, and inversion will continue to make the technique more attractive.

Cardiff et al. (2013b) first suggested a modified approach named oscillatory hydraulic tomography (OHT), in which periodic pumping tests are used as the

[1]Department of Geoscience, University of Wisconsin-Madison, 1215 W. Dayton St., Madison, WI, 53711.
[2]Corresponding author: Department of Geoscience, University of Wisconsin-Madison, 1215 W. Dayton St., Madison, WI 53711; cardiff@wisc.edu
[3]School of Earth Sciences, The Ohio State University, 275 Mendenhall Lab, 125 South Oval Mall, Columbus, OH, 43210.
[4]Department of Geosciences, Boise State University, 1910 University Drive, Boise, ID, 83725.
[5]Department of Civil and Environmental Engineering, Building, 473 Via Ortega Room 311, Stanford University, Stanford, CA, 94305.

Article impact statement: Oscillating pumping tests are demonstrated at the field scale as a method for minimally invasive aquifer heterogeneity imaging.

Received April 2019, accepted October 2019.

doi: 10.1111/gwat.12960

aquifer stimulation or "source," and pressure transducer "receivers" are used to record the change in amplitude and phase of the oscillating signal at different locations within the aquifer. The data collected during an OHT survey can be processed using spectral methods and can be efficiently inverted using a phase-domain or "steady periodic" numerical model, which eliminates the need to specify time-stepping or other transient model parameters.

Following initial numerical investigations, the technique of OHT has been applied in laboratory sandbox settings. Zhou et al. (2016) investigated the ability of OHT to image aquifer heterogeneity in a sandbox while examining the resolution and accuracy of tomograms obtained across a range of source and receiver densities. Zhou and Cardiff (2017) similarly investigated the ability of OHT to monitor changes in "effective" hydraulic conductivity as fluids with different viscosities and densities migrated within a sandbox. In both of these works, the sediments used in packing the sandbox were uniform across its thickness, making all of the experiments effectively two-dimensional (2D) in nature.

In this work, we describe field implementation of OHT in three dimensions (3D), in the manner described by Cardiff et al. (2013b) (i.e., a survey consisting of oscillating pumping tests with data inverted via a phase-domain model). Although we believe this is the first fully tomographic field implementation of 3D OHT, several previous works have implemented oscillatory tests in the field and processed the data to infer aquifer properties. Lavenue and de Marsily (2001) collected data during several oscillating pumping tests performed in the Culebra dolomite of New Mexico. Their observational network consisted of seven wells with two discrete depths isolated in each well. In analyzing the data, they utilized a two-layer transient numerical model with heterogeneity parameterized via pilot points. Renner and Messar (2006) performed oscillatory pumping tests across a range of periods from 10 to 5400 s at a three-well site in Bochum, Germany. Data from these experiments were analyzed using a set of analytical solutions that assume homogeneous aquifer properties. In a project report, McElwee et al. (2011) explored an application of oscillatory testing at 30 s periods applied at the well-known GEMS site in Kansas, which were analyzed primarily with a physically-approximate "ray-based" model. Recently, Fischer et al. (2018) analyzed data from a set of four oscillatory pumping tests at the fractured karstic Lez aquifer in France. Using data from 13 observation boreholes, they implemented a 2D numerical model within a cellular automata-based inversion that detected karstic network structure.

In this work, we analyze data from a series of oscillatory pumping tests conducted in 2013 at the Boise Hydrogeophysical Research Site (BHRS) in Boise, Idaho, USA. The full field campaign consisted of oscillating pumping tests performed at three different depths in each of two different wells, monitored by a total of 25 discrete zones within three observation boreholes. These tests are the same as those described by Rabinovich et al. (2015), where an effective-media analytical model was used to analyze a subset of the records individually (i.e., nonjointly). Here, we jointly analyze a subset of the recorded tests using a phase-domain numerical forward model within a geostatistical inversion approach. Relative to the existing works described above, this analysis represents the first truly 3D tomographic analysis of oscillatory pumping test data that we are aware of. In addition, this work provides data, data processing routines, and computer code for the analyses as Supporting Information S3, which may be utilized by other researchers interested in the OHT approach.

Field Site and Experimental Data Collection

The Boise Hydrogeophysical Research Site (BHRS) is a field research site operated by Boise State University and located approximately 15 km southeast of downtown Boise, Idaho, USA, near the coordinates N43.542322 W116.097687. Located on a gravel bar adjacent to the Boise River, the BHRS provides a testbed for investigation of hydrogeologic properties and processes with infrastructure including 18 fully screened wells, several piezometers, and river stage gauges. Initial hydrogeologic investigations showed that the aquifer at the site, approximately 20-m thick, consists of sand to sand-and-gravel deposits with relatively high hydraulic conductivity and moderate variability (Barrash and Clemo 2002; Barrash and Reboulet 2004; Barrash et al. 2006). The site is underlain by a clay aquitard that is partially overlain by the thin edge of a basalt flow; all wells terminate in the clay. The site's setting adjacent to the Boise River provides a convenient boundary condition, where river levels are highly regulated by two dams—Diversion Dam, located approximately 600-m upstream, and Lucky Peak Dam, located approximately 5-km upstream.

Field experimentation at the BHRS has included numerous hydraulic and geophysical experiments in an effort to constrain relevant subsurface properties (hydraulic conductivity, porosity, specific storage, specific yield), as well as to map correlations between different hydraulic properties and between hydrologic and geophysical properties. Of particular relevance to this work, 3D HT experiments have been performed under two different configurations at the BHRS in 2011 (Cardiff et al. 2012) and 2012 (Cardiff et al. 2013a). Likewise hydraulic conductivity was estimated near boreholes through a comprehensive series of slug tests (Barrash and Cardiff 2013; Cardiff et al. 2011).

To provide context for the data and results described in this work, we briefly revisit the test datasets from the 2011 and 2012 HT field experiments, which will serve as a basis for comparison in later discussions. In 2011, a HT experiment was performed in which a series of pumping tests were carried out at wells B4 and B5, at successive 1-m intervals within each well. Drawdown was monitored at four observation wells (B1, B2, C3, and C4) using packer-and-port strings with 2-m interval

separations between monitoring zone centers. As a simple method of data compression, three data points from each drawdown curve were selected for fitting, for a total of 796 drawdown observations inverted (Cardiff et al. 2012). In 2012, a second HT campaign was performed consisting of a series of pumping tests performed at well B1, with five wells (B3, C3, C4, C5, and C6) monitored. In this case, the maximum distance between pumping and observation wells was 12.3 m. Successive 1-m intervals were pumped, and responses were measured using packer-and-port strings with 2-m interval separations between monitoring zone centers. After performing all pumping tests, the packer-and-port strings were shifted by 1 m and the pumping tests were repeated, such that each test had an effective observation density of 1 m. Again, three drawdown observations per individual drawdown curve were inverted, resulting in a total of 2628 observations inverted (Cardiff et al. 2013a).

The experiments analyzed in the current work were designed as a proof of concept for OHT. Similar to other HT studies described at the BHRS, during OHT a hydraulic "stress" was applied at a given location and depth in the aquifer—in this case, oscillatory pumping—and the resulting head changes at a number of monitoring locations are the data available for analysis. The OHT experimentation took place during a field campaign in July 2013. Figure 1 highlights the locations of wells, pumping intervals, observation intervals, and packers used during the OHT testing. A custom-designed oscillating signal generator (OSG)—consisting of a down-hole piston connected to a surface piston by hydraulic lines, and with a maximum total cycling volume of 2 L—produced the pumping signal for all experiments. To drive the motion of the down-hole piston, a motor at the land surface was connected to a flywheel which rotated at a set speed. The rotational motion was translated into linear motion of the surface piston by a connecting arm (Figure 2). By changing the position of the connecting arm on the flywheel (i.e., the radius of rotation) and the speed of the motor, both the cycling volume and the frequency of the piston movement could be altered. During testing in the field, the apparatus could achieve an effective period range of between approximately 90 and 10 s, with a total cycled fluid volume of between 1.5 and 0.4 L.

Monitoring of aquifer head changes was achieved with temporary borehole equipment. A set of packer installations—consisting of nominal 1-m monitoring zones separated by 1-m flexible rubber packers—were inserted in wells B1, B4, and C4 (locations labeled in blue, Figure 1). Each installation consisted of between seven and nine monitoring zones per well and allowed measurement of head changes at discrete depths within each well. Fiber-optic pressure transducers were inserted into ports accessing each monitoring zone, and all were connected to a centralized data acquisition (DAQ) system, allowing reliable simultaneous measurement and visualization of head changes in all zones (Figure 2).

In addition to the above testing and monitoring arrangements, we placed three packers in each of four

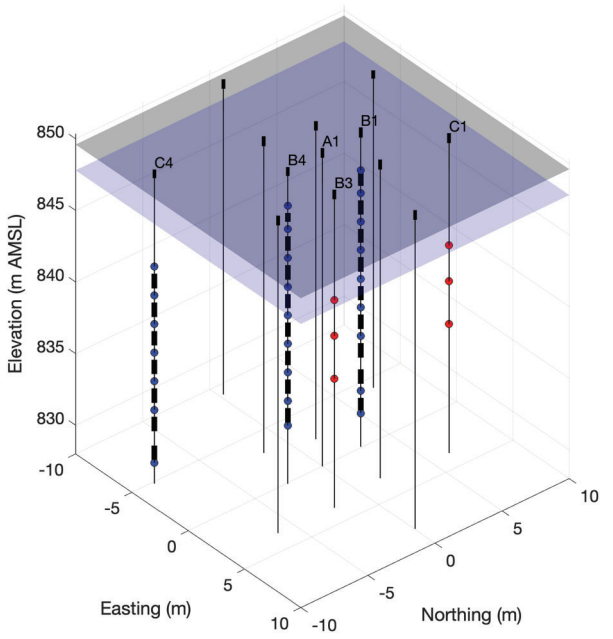

Figure 1. BHRS central wellfield. Well A1 (center of field) represents origin, with labeled wells representing those used in OHT experiments. Red and blue points represent pumping and observation locations, respectively, with packer locations shown in black. Planes represent land surface and approximate location of water table.

wells (A1, B2, B5, and B6) in the middle of the wellfield that were not used in the HT testing to reduce the possibility of head equalization in open wells. Head changes during HT tests were not monitored in these zones, but daily checks on packer inflation confirmed continual blockage of head integration through these wells.

At the beginning of an OHT test, the DAQ system was initialized and test files were automatically saved, recording the spatial arrangement of pressure transducers, transducer scaling parameters, and all other inputs assigned via the DAQ system's software. Live signals from all transducers were then visualized. Once transducer readings were observed to have stabilized, the offsets for all transducers were reset such that records were centered around an initial value of zero head change. Recording of pressure measurements then began, at a nominal frequency of 125 Hz. After several seconds, the OSG motor was started and the desired speed of oscillations was set. Head changes in response to the piston motion were recorded continuously until at least five complete periods of consistent head change oscillations were observed. Throughout testing, live visualization of all transducer readings allowed for experimental issues to be assessed and noted quickly (e.g., due to a transducer accidentally shifting position during testing).

Locations used for oscillatory pumping are labeled in red in Figure 1, and displayed along with locations of monitoring interval centers (blue points). The locations of all testing apparatus and additional site spatial information are included as Supporting Information S2. The particular series of tests performed consisted of a range of different

Figure 2. Field photographs from OHT application. Clockwise from upper-left: Surface motor and attachment to surface piston; hydraulic pressure lines entering pumped well; fiber optic pressure transducers attached to light source; field data acquisition of all data on laptop.

periods of oscillation, which is documented in Table 1. A subset of example data collected during two of the tests is shown in Figure 3. Thanks to the high-accuracy fiber-optic pressure transducers used (FISO Model FOP-MIV-NS-369), signals with an amplitude of 1 to 2 mm are clearly discernable and display consistent amplitude and phase. As demonstrated in Figure 3, discernable oscillatory signals were observed at distances approaching 20 m from the oscillating pumping location. In these figures, as in many sets of raw data, we note that the recorded signals are not perfectly symmetrical or sinusoidal. Based on observations of head changes within the pumping well, it appears that this asymmetry was caused by the OSG producing an input signal that was not perfectly sinusoidal.

Analysis Methodology

As mentioned in Bakhos et al. (2014), oscillatory signals with a constant frequency can be extracted quickly and relatively easily—even from noisy transient data—by the use of fast Fourier transform (FFT) data processing. Such an approach was demonstrated at the sandbox scale in Zhou et al. (2016). In this work, we apply a similar and largely automated workflow to field data from the BHRS.

Data processing proceeded in a step-wise fashion, which included: (1) Initial importing of the main text file records into MATLAB binary files; (2) Manual visualization, removal of incomplete/low-quality tests, and resampling of high-quality tests; (3) Extraction of phasors (i.e., signal phases and amplitudes) from all pressure signals; (4) Summarization and visualization of phasor metrics based on results of steps 1–3 for initial quality assurance (QA); (5) Formation of data vectors for inversion and forward model setup; (6) Setup of inversion data error metrics, regularization parameters, and running of inverse modeling code; and (7) Postinversion visualization.

An open question in hydrogeologic research (and indeed, many tomographic fields) has been the degree to which choices involved during data processing and inversion affect the ending output of tomographic results. In an effort to help answer this question, and to make our data analysis as transparent and reproducible as possible, we provide all raw data collected, all data processing scripts, and all inverse modeling functions as Supporting Information S3 to this manuscript. While we describe what we believe to be the reasonable choices we have made in processing our data in the following paragraphs, the interested reader may test the impacts of different analysis approaches and assumptions using our code. Each step in the data processing is represented by its own MATLAB script. User-defined analysis parameters that may be altered are defined prominently at the beginning of each script, so that they may be easily seen and changed. For the results presented herein, we briefly describe the analysis choices made during each data processing step here.

Processing of the head change data proceeded as follows. In Step 1, the data from all test files are imported into MATLAB binary files (variables) with timing information converted to time in seconds after the start of the datafile. No other major analysis choices are associated with this step. In Step 2, tests from the campaign were removed from consideration if they represented tests that were cut short due to instrument malfunctions or other issues. The pressure records from

Table 1
Test Data Files Selected for Analysis after Initial Manual Filtering

Test Filename	Stroke Volume (Liters)	Oscillation Well	Oscillation Zone Elev. (m)	Dominant Period (s)	Length of Trimmed Signal (s)
07122013_test1	1.42	B3	837	73.01	587
07122013_test2	1.42	B3	837	46.93	470
07122013_test3	1.42	B3	837	64.74	518
07122013_test4	1.42	B3	837	29.62	503
07152013_test4	1.42	B3	840	69.34	417
07152013_test5	1.42	B3	840	46.80	516
07152013_test6	1.42	B3	840	40.04	361
07152013_test7	1.42	B3	840	28.60	514
07162013_test1	0.45	B3	837	22.62	272
07162013_test2	0.45	B3	837	17.72	372
07172013_test1	0.45	B3	837	23.70	355
07172013_test2	0.45	B3	837	14.95	223
07172013_test3	0.45	B3	837	9.78	274
07172013_test4	0.45	B3	840	24.12	410
07172013_test5	0.45	B3	840	18.23	401
07172013_test6	0.45	B3	840	13.53	122
07172013_test7	0.45	B3	840	9.48	265
07172013_test8	0.45	B3	842.5	24.03	337
07172013_test9	0.45	B3	842.5	18.16	272
07172013_test10	0.45	B3	842.5	13.79	151
07172013_test11	0.45	B3	842.5	9.54	296
07192013_test1	0.45	C1	837	24.40	400
07192013_test2	0.45	C1	837	18.67	355
07192013_test3	0.45	C1	837	13.97	307
07192013_test4	0.45	C1	837	9.79	205
07192013_test5	0.45	C1	840	24.26	340
07192013_test6	0.45	C1	840	18.38	128
07192013_test7	0.45	C1	840	18.20	182
07192013_test8	0.45	C1	840	13.82	165
07192013_test9	0.45	C1	840	9.71	194
07192013_test10	0.45	C1	842.5	23.34	233
07192013_test11	0.45	C1	842.5	17.84	237
07192013_test12	0.45	C1	842.5	13.46	176
07192013_test13	0.45	C1	842.5	9.60	144

Note: Trimmed sections of data were selected from full raw record based on times when all observed channels appeared to produce consistent amplitude and phase of oscillations.

the remaining tests were then trimmed (to remove the transient phase, at the start and end of a test, when head oscillation amplitudes or phases are nonconstant) and resampled to a uniform 0.1 s time interval to correct for inconsistency in the DAQ system sampling rate. Finally, the signals were corrected for atmospheric pressure changes. As with any hydraulic characterization, initial manual visualization of all transducers is essential in order to address field hardware issues that can affect responses, such as crimped pass-through tubing or poorly inflated packers. This step next removed specific observations or full tests from consideration based on these visualizations. In the analysis presented here, the records that were not further analyzed and the reasoning was recorded in an associated spreadsheet included as Supporting Information S1, which was produced during manual visualization of time-series data. A total of 52 test datafiles were recorded, and during a first round of screening, 10 tests were removed from consideration. These removed tests included obvious "false start" cases where a test was cut short after a few oscillation periods, or where other technical difficulties occurred. During a second round of screening, eight additional tests were removed due to indications that the packers associated with the pumping zone were not adequately inflated. For the remaining 34 tests that passed screening, time intervals were selected denoting the portion of the recorded signal that was trimmed and analyzed further. These time intervals were selected such that several periods of oscillation were present, and that: (1) the first five periods of oscillation were excluded, such that steady-periodic conditions were likely; (2) all observation channels showed stable behavior (e.g., no unexpected "jumps" in pressure transducer readings); and (3) the last two periods of oscillation were excluded, to eliminate the use of any "ramp-down" oscillations that may have occurred at the end of each test. At the completion of Steps 1 and 2, the data in MATLAB matrices contain processed steady-periodic pressure data from all tests that passed screening, with uniform sampling intervals and atmospheric effects removed.

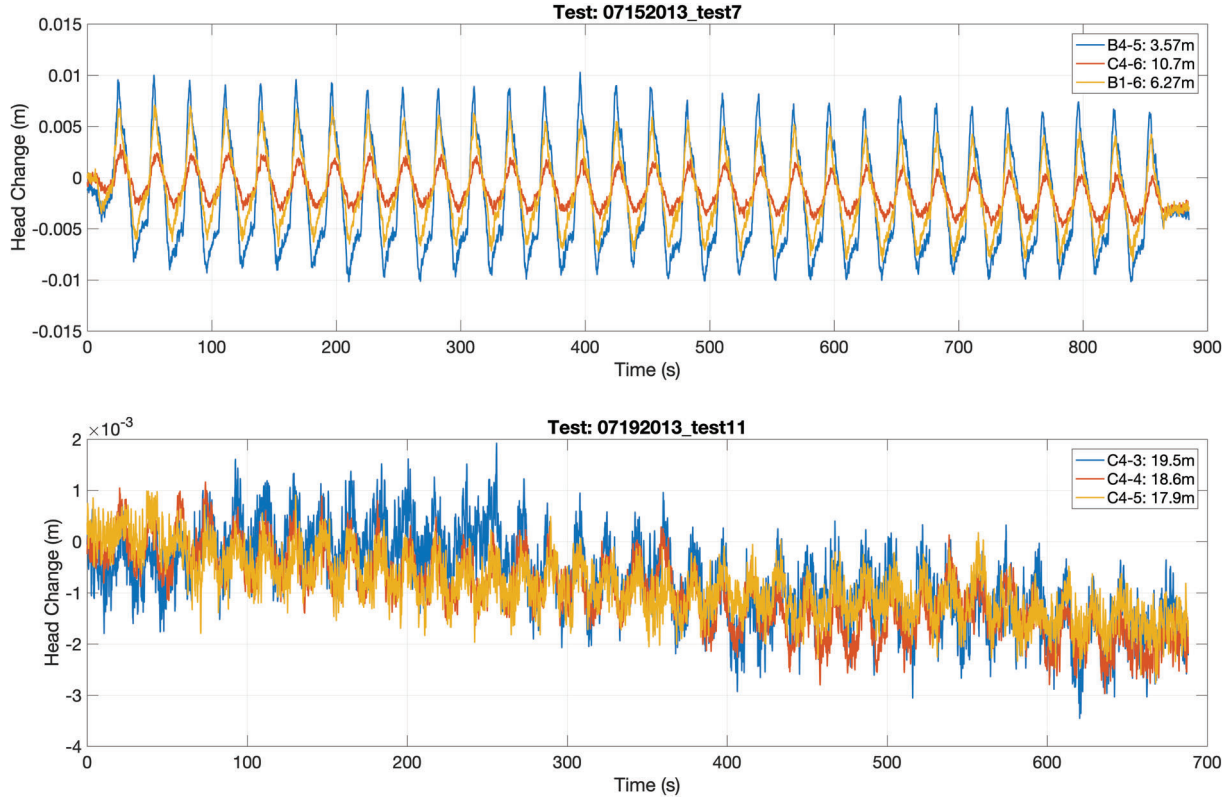

Figure 3. Example raw data from OHT testing. Top: Example data with well B3 pumping at 840-m elevation AMSL, with plotted channels representing those closest to 840-m elevation in surrounding observation wells. Bottom: Submillimeter oscillating head changes observed (note vertical axis) in well C4 during pumping at well C1. In this case, all plotted transducers are >15 m from the pumping location.

The processed data from Step 3 meets all requirements for signal processing using the discrete Fourier transforms. During Step 3, the FFT is first applied to data from the pumping zone associated with each test, which allows us to determine the exact period at which aquifer stresses were applied. This information, unfortunately, could not be recorded independently with the specific OSG used in this study, necessitating this analysis approach. After FFT processing, dominant peaks in the Fourier spectrum of the pumping interval head signals (and their associated frequencies) are extracted automatically. In our particular analysis, we extracted only the two most dominant peaks, though this is an adjustable parameter in the provided scripts. Because the FFT is a discrete Fourier transform—limited to returning Fourier coefficients (phasors) for a discrete set of frequencies—it is possible that the peaks in an FFT-based signal spectrum may not represent the exact pumping frequency. For this reason, estimates of dominant frequencies and their associated phasor coefficients were updated by performing least-squares optimization against the pumping zone data, as follows:

$$\min_{\substack{A_d,\,B_d,\,\omega_d\\ A_s,\,B_s,\,\omega_s}} \sum_{i=1}^{n} \left(h(t_i) - \left(A_d \cos(\omega_d t_i) - B_d \sin(\omega_d t_i)\right.\right.$$
$$\left.\left. + A_s \cos(\omega_s t_i) - B_s \sin(\omega_s t_i)\right)^2 \right. \quad (1)$$

where $h(t_i)$ $[L]$ represents the head measurement at time t_i $[T]$, ω_d, ω_s $[T^{-1}]$ represent the angular frequencies of the dominant and secondary period, and (A_d, B_d), (A_s, B_s) represent the real and imaginary components of the phasors associated with the dominant and secondary frequencies, respectively. A secondary frequency was included in our data fitting approach because of the signal produced by the OSG, which was not perfectly sinusoidal. Minimization was carried out using the Nelder-Mead simplex algorithm –implemented in MATLAB as `fminsearch`—using the results from FFT processing as initial guesses for all parameters. In all cases, the updates to the estimated phasor coefficients and frequencies were small, but produced some improvement in reducing total squared misfit. After this processing in Step 3, phasor coefficients were extracted from all test observations, and the results (frequencies of testing and associated phasor measurements) are visualized using our Step 4 script. This step allows plotting of phasor changes as a function of location within the aquifer and distance from the pumping interval. An example of this visualization is shown in Figure 4.

Following data processing and extraction of signal phasors, the remaining steps for performing OHT are to set up numerical "forward" models capable of simulating the field testing regime, and to use these forward models to iteratively update parameter estimates within an inversion framework. During Step 5, all inputs necessary to set

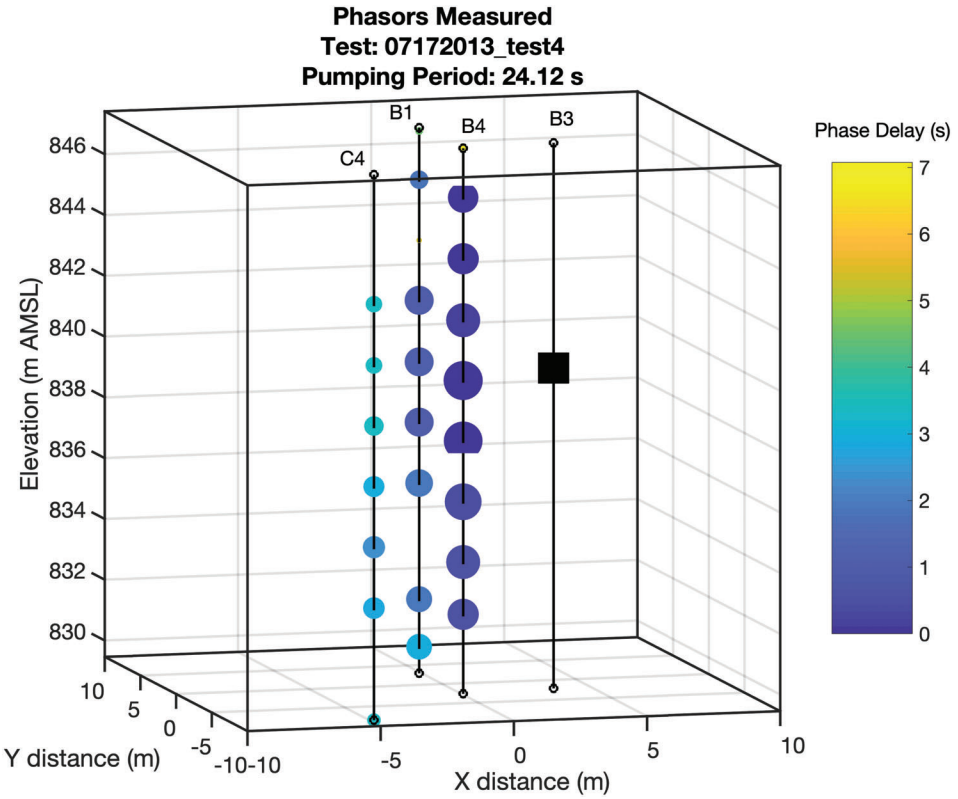

Figure 4. Visualization of measured signals from one pumping test. Black square represents location of pumping interval. Circles represent observed signals: sizes are proportional to amplitude of signal, and colors reflect phase delay of signal in seconds relative to first response.

up the forward model simulations are defined. These inputs include: (1) The domain: the size, discretization, and boundary conditions for the modeled region; (2) The "sources": the series of oscillating pumping tests to be simulated (frequencies, amplitudes, and pumping locations); and (3) The "receivers": locations at which observations of the oscillating test's induced head changes should be recorded. Observations that should be excluded from simulation in the forward model are also defined at this stage. For example, the user may choose that only a certain subset of the tests is simulated, or that particular observations are excluded. In our analysis, we selected data from the tests performed on July 17, 2013 and July 19, 2013, and exclude secondary frequency components from inversion due to the fact that this secondary signal is poorly constrained. Whereas the pumping at the dominant frequency is known to have a total cycled volume of 0.446 L for all of these tests (based on the known volume of the piston and stroke length during testing), the magnitude of the volume cycled at this secondary period is unknown. In our results, we also excluded monitoring zones that were below the depth of 830 m, where we have placed the bottom boundary of our numerical model. Many areas below ~831-m depth are known to be within a clay aquitard—as observed in drill core and other site characterization.

Analysis of the collected data (i.e., oscillating signal amplitudes) is carried out using a MATLAB-based numerical forward model that simulates groundwater head changes in the "steady-periodic" or phase domain. As described in Cardiff et al. (2013b), this model simulates the amplitude and phase of head changes within the modeled domain by solving the governing equation for the head phasor, which is derived from the confined groundwater flow equation:

$$i\omega S_s \Phi = \nabla \cdot (K \nabla \Phi) + Q_\omega \tag{2}$$

where Φ $[L]$ is the complex head phasor associated with pumping frequency ω $[T^{-1}]$, K $[LT^{-1}]$ is hydraulic conductivity, S_s $[L^{-1}]$ is specific storage, Q_ω $[T^{-1}]$ represents the phasor of the volumetric fluid source, and i is the imaginary unit. Boundary conditions allowed for our model include no-flow boundaries and boundaries of no head change, that is, $\Phi = 0$. Q_ω and Φ can be converted back to time-domain pumping rates and head changes as:

$$Q(\boldsymbol{x}, t) = Re[Q_\omega(\boldsymbol{x}) \exp(i\omega t)] \tag{3}$$

$$h(\boldsymbol{x}, t) = Re[\Phi(\mathbf{x}) \exp(i\omega t)] \tag{4}$$

Step 6 of the data processing sets up all parameters necessary to begin inverse modeling of the field data, and then runs the geostatistical inversion approach as documented in (Cardiff et al. 2012). The parameters defined in this step include assumed data error contained in the

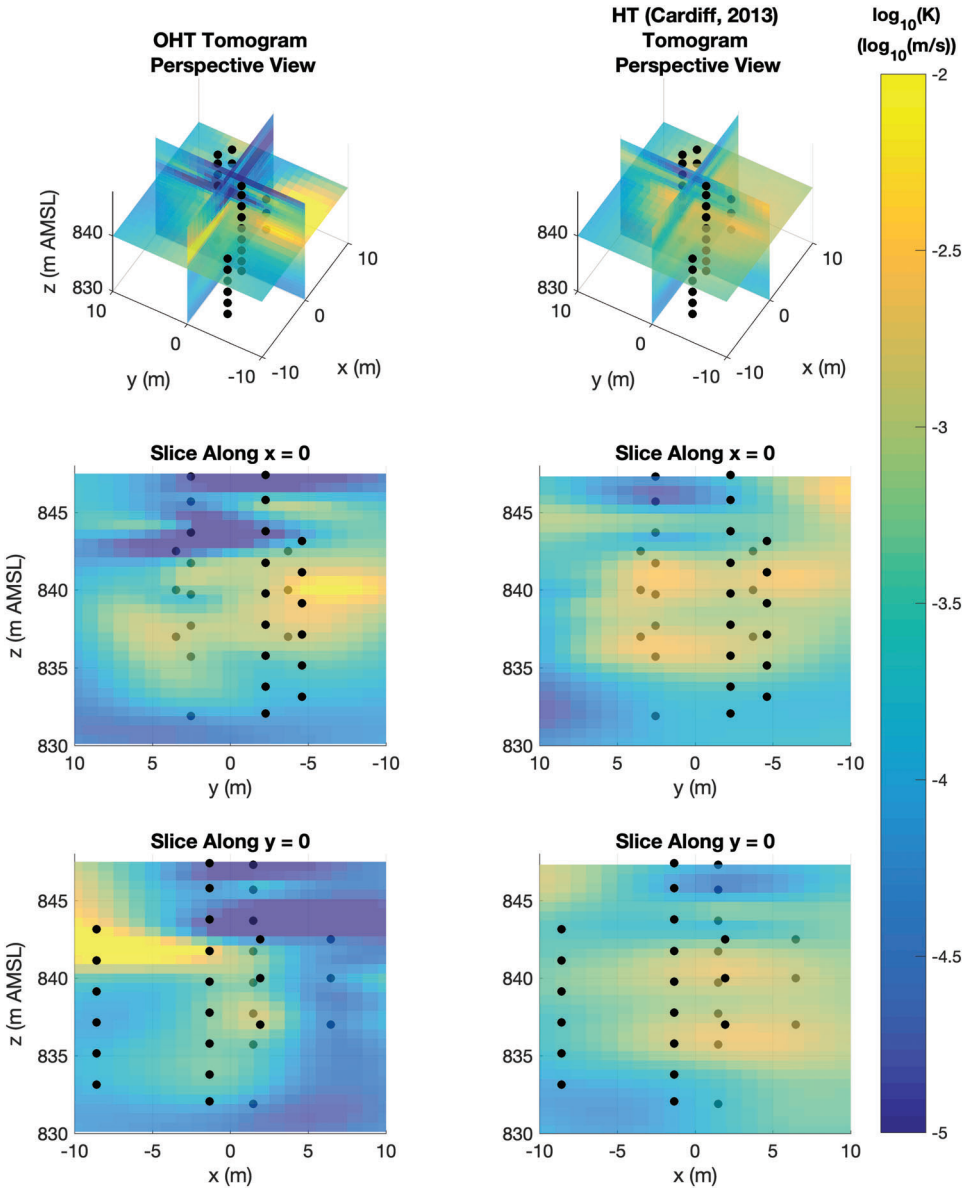

Figure 5. Comparison of tomograms between current OHT inversion (Case 1) and prior HT inversion (Cardiff et al. 2013a). Black dots represent locations of centers of pumping and observation zones.

time-series signal, geostatistical parameters assumed as part of the geostatistical inversion, and initial (homogeneous) parameter values assumed as a starting point in the inversion. The results of inverse modeling are produced at the completion of Step 6. In Step 7, these results are visualized through: (1) comparison (i.e., cross-plots) between observed field data and data simulated by the final heterogeneous numerical model; (2) visualization of the 3D parameter estimates via tomogram slices; and (3) comparison between inverted hydraulic conductivity values obtained in this study and values obtained from previous studies at the BHRS.

Field Data Analysis

The numerical model setup for forward and inverse modeling is described by the parameters in Table 2. Lateral boundaries at X/Y locations located 30 m from the central well (A1) were set as no head change boundaries. The impact of these boundaries was examined by testing the numerical model at several lateral sizes and ensuring that boundary locations resulted in minimal changes to signal amplitudes at observation locations. Similarly, other discretization-based impacts such as the size of individual model grid cells were investigated during early model development, in order to ensure model accuracy while striking a balance in computational effort. Vertical boundaries, at the lower aquitard and near the water table, were set as no-flow boundaries. In order to experiment with the impact of storage conditions near the water table, we utilized two alternative conceptual models. In the first case, a compressive specific storage value of $S_s = 10^{-5}[m^{-1}]$ was used throughout the model domain, representing a typical compressive storage value for the

Table 2
Parameters Used in Setup of Numerical Phase-Domain Forward Model

Parameter		Value	Units
Rotation angle from North to model Y axis		32	Degrees CCW
X discretization	Min. value	−30	m
	Max. value	30	m
	Discretization	1	m
Y discretization	Min. value	−30	m
	Max. value	30	m
	Discretization	1	m
Z discretization	Min. value	829.8	m AMSL
	Max. value	847.8	m AMSL
	Discretization	0.6	m
Boundaries	At X min	0	m head change
	At X max	0	m head change
	At Y min	0	m head change
	At Y max	0	m head change
	At Z min	0	m^3/s flux
	At Z max	0	m^3/s flux

Table 3
Parameters Used in Setup of Geostatistical Inversion Routines

Parameter	Value	Units
S_s value (constant)	1E-05	1/m
S_y (top layer, if used)	0.03	[−]
$ln(K)$ initial guess	−9	ln([m/s])
$ln(K)$ variance	0.5	[−]
L_x	6	m
L_y	6	m
L_z	1.2	m

BHRS based on prior site investigations. In the second case, the model layer closest to the surface was given a specific storage value equal to S_y/b, where specific yield $S_y = 0.03[-]$, a representative value for the BHRS for short-duration pumping tests (Barrash et al. 2006), and $b = 0.6[m]$, the thickness of the top-most model layer. This approximate method for simulating storage in the top-most layer assumes that fast saturation/desaturation occurs within this region in response to pressure changes near the water table, and likewise assumes that the change in saturated thickness of the aquifer is small relative to total saturated thickness. The former assumption is supported by earlier testing at the BHRS that exhibited fast drainage response during pumping tests (Barrash et al. 2006). That said, the response of unconfined aquifers, broadly, at shorter timescales such as the ∼10 s periods employed in our testing is an area of ongoing research. The latter assumption is likely valid for these tests at the BHRS, which has a total thickness of >10 m and experienced maximum head changes (at pumping intervals) commonly of 5-10 cm throughout OHT testing.

Phasors of head change within the model domain were simulated at each individual testing frequency, and for each individual pumping location. The numerical model setup and solution are implemented via a modified version of the MATLAB code used by Zhou et al. (2016); the code is provided as part of Supporting Information S3 for this manuscript. This new version of the code is designed to accept inputs in a user-friendly fashion and includes adjoint state capabilities for calculating model sensitivity Jacobians (see, e.g., the mathematical description in Cardiff et al. 2013b), as well as optional inputs for choosing the types of linear system matrix solvers applied.

For inversion, we used the quasi-linear geostatistical approach pioneered by Kitanidis (1995). An exponential variogram was assumed as the geostatistical "prior" during inversion, with the correlation lengths and variances specified according to Table 3. The geostatistical parameters assumed represent those obtained for the BHRS after analysis of a series of slug tests, as described in Cardiff et al. (2011). Temporal data error in measured signals was initially assumed at $\sigma_t = 1\ mm$, based on the stated accuracy of the fiberoptic pressure transducers used (FISO Model FOP-MIV-NS-369). This error was translated, before inversion, to an estimate of expected error for oscillatory signal amplitude observations, following the linear error propagation approach described in Bakhos et al. (2014).

Our code is parallelized to allow both shared-memory and distributed-memory performance of inversion tasks. However, to provide a benchmark that is relevant to users without significant computational resources, we performed all inversion on a standard desktop PC. The inversions discussed below were performed on a Dell XPS 8930 Windows PC (8th Gen Core i7 Intel 6-core CPU) with 16 GB of RAM. As with most inversions, the single most computationally intensive step is the calculation of simulated observations' sensitivity to individual model parameters, that is, evaluation of the Jacobian. In the most computationally intensive case described below (108,000 estimated K values, and 552 observations of head change magnitude), evaluation of the full model Jacobian required under 30 min of computational time. The quasilinear geostatistical inversion routine iteratively performed forward model runs and Jacobian updates to progressively reduce the value of the geostatistical objective function, formulated as:

$$\min_{s,\beta} \frac{1}{2}(\boldsymbol{y} - \boldsymbol{h}(\boldsymbol{s}))^T \boldsymbol{R}^{-1}(\boldsymbol{y} - \boldsymbol{h}(\boldsymbol{s})) + \frac{1}{2}(\boldsymbol{s} - \boldsymbol{X}\beta)^T \boldsymbol{Q}^{-1}(\boldsymbol{s} - \boldsymbol{X}\beta) \quad (5)$$

where $\boldsymbol{y}$ $(n \times 1)$ is a vector of observed data, $\boldsymbol{s}$ $(m \times 1)$ is a vector of model parameters, $\boldsymbol{h}()$ is the numerical forward model which accepts parameters as input and produces predicted observations, $\boldsymbol{R}$ $(n \times n)$ is a covariance matrix for expected data errors, $\boldsymbol{X}$ $(m \times 1)$ is a vector of ones, $\boldsymbol{\beta}$ is the scalar mean of the parameters, and $\boldsymbol{Q}$ $(m \times m)$ is

Table 4
Correlation of K Values Obtained via OHT Compared Against K Values Estimated via HT Analyzed in Cardiff et al. (2013a)

Case	Tests Inverted	Data Error σ Assumed [m]	Top Layer Storage	Correlation coefficient: B-Well Profiles (B1, B3, B4)	All OHT Well Profiles(B1, B3, B4, C1, C4)	Central Grid (10 m x 10 m)	Well Profiles (All Wells)	Full Grid (30 m x 30 m)
1	*B3, C1*	*0.003*	*Sy/Δz*	0.603	0.502	0.546	0.454	0.414
2	*B3*	*0.003*	*Sy/Δz*	0.446	0.345	0.403	0.350	0.295
3	*B3, C1*	*0.001*	*Sy/Δz*	0.404	0.388	0.314	0.287	0.341
4	*B3*	*0.001*	*Sy/Δz*	0.318	0.356	0.317	0.246	0.317
5	*B3, C1*	*0.001*	*Ss*	0.395	0.390	0.302	0.281	0.326
6	*B3*	*0.001*	*Ss*	0.289	0.332	0.291	0.238	0.309

Note: Rows represent different inversions of OHT data. Correlation coefficients in columns represent different portions of the K field being correlated.

an expected covariance matrix for the model parameters, as determined by the spatial variogram.

Further details on the quasilinear geostatistical approach to inversion, as implemented here, can be found in, for example, Cardiff et al. (2009). Convergence was declared when both: (1) The largest relative change in the parameters was less than 0.001 between iterations; and (2) The relative decrease in the objective function was less than 0.001 between iterations. Total inversion time to achieve convergence was typically several days, but always less than 1 week.

Results

Several inversions of the OHT field data were performed, in order to assess the impacts of different forward and inverse modeling assumptions on the obtained characterization results, as presented in the rows of Table 4. The results presented assessed the impact of three factors: (1) The inclusion of data from multiple pumping wells (i.e., B3 and C1) vs. only a single pumping well (B3); (2) the assumption of compressive storage at the top of the numerical model vs. assuming water table (draining) storage; and (3) the assumption of data error that is determined only by the magnitude of the stated sensor measurement resolution vs. an assumption of larger data errors reflecting, for example, additional numerical and conceptual modeling errors. Examples of tomographic results and data fit for our preferred case (Case 1) are shown in Figures 5 and 6, respectively. For this case, the root mean squared (RMS) difference between simulated and observed data is approximately 0.2 mm.

As a basis for assessing the impacts of different inverse modeling assumptions, we calculated correlation coefficients between the K values estimated via OHT throughout the BHRS volume against K values estimated through earlier (nonoscillatory) 2012 HT experiments at the site (Cardiff et al. 2013a). Both datasets are subject to the uncertainty and resolution limitations associated with all tomographic approaches. However, as the two sets of results relied on different testing geometries and pumping

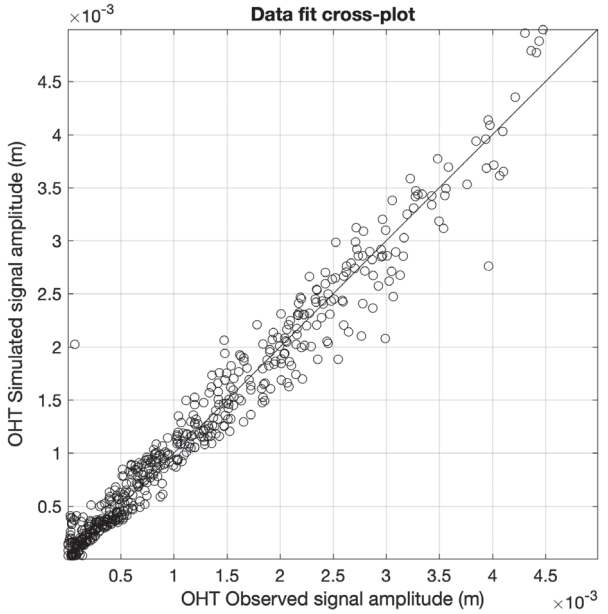

Figure 6. Data fit between observed and simulated oscillation amplitudes (Case 1).

test styles, correlation between K estimates from these two datasets represents a largely independent validation of the parameter estimates obtained via the two separate methods.

The sensitivity of all HT methods is known to be strongest closest to monitoring and pumping locations. For this reason, we investigated the correspondence between K profiles obtained via both HT and OHT methods at the location of the B-wells used for pumping or monitoring during the OHT tests. These profiles, shown in Figure 7, show similar values and trends in K values measured by OHT and HT, and are most consistent in the region around 842 m and below. All OHT pumping zones were below the depth of 842 m, and similarly many of the observation zones are found below this level, which may explain the improved consistency in this region. In terms of quantitative comparison, the K profiles for the

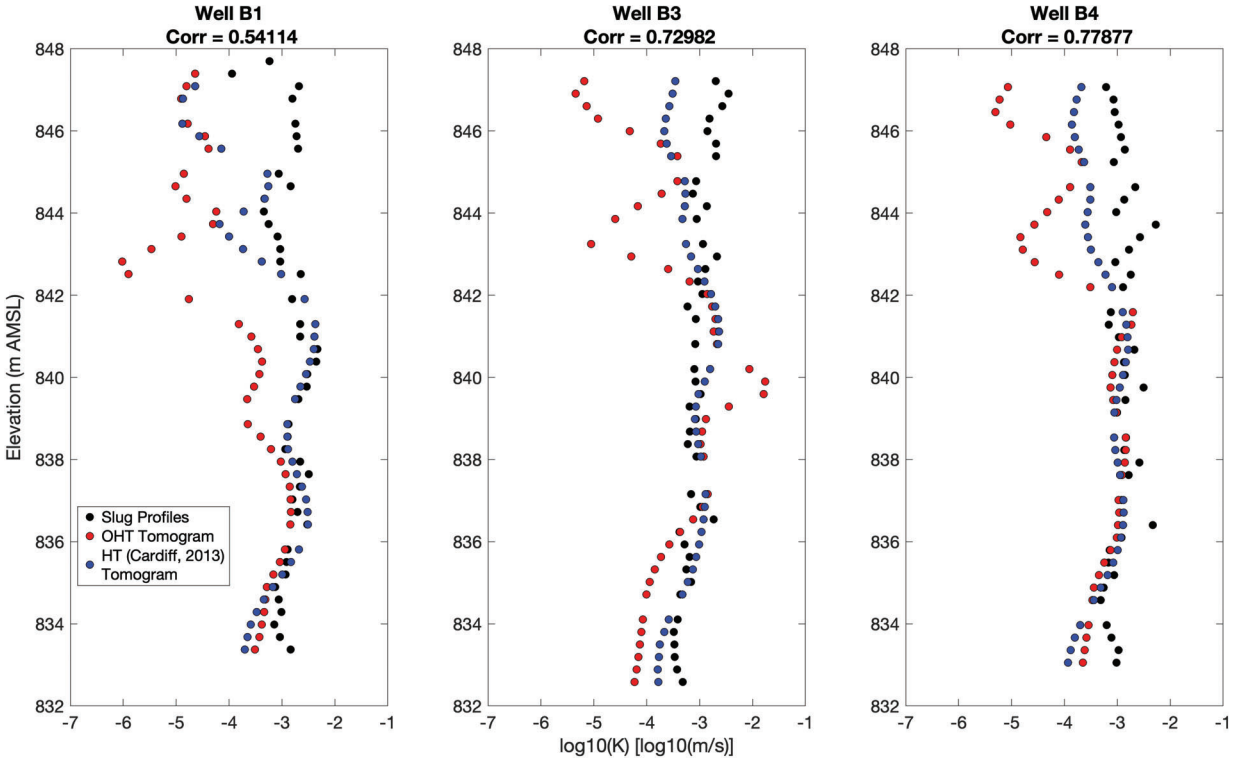

Figure 7. Comparison between K profiles for central wells B-wells used in OHT testing. Comparison between OHT (this work, Case 1), slug testing results (Barrash and Cardiff 2013), and hydraulic tomography (HT) (Cardiff et al. 2013a).

B-wells demonstrate moderate correlations (correlation coefficient >0.5, B1) to strong correlations (correlation coefficient >0.7, B3 and B4), indicating that OHT is able to produce high-quality K estimates at the center of the investigated aquifer volume. That said, this region represents the location where data density is highest and the best characterization results should be expected.

To further investigate the reliability of OHT K characterization, we present K correlation results between OHT inversions and the earlier 2012 HT dataset for a variety of different subsets of the data in Table 4. The columns of the table in this case can be thought of as assessing the correlation between the two K fields within different subregions of the imaged aquifer. Several consistent trends in these correlations can be gleaned from this table.

First, it is apparent that regardless of other parameters, and regardless of correlation metric chosen, that the inclusion of the additional pumping tests at well C1 result in improvement of the imaged K field. In almost all cases, correlations with the pre-existing 2011 HT data were improved by using both the B3 and C1 pumping tests, rather than just pumping tests at well B3. This result is perhaps not unexpected—as more data should indeed provide more accurate imaging results—but shows confirmation that the performance of OHT at field scales can be improved as greater instrumentation is added (Cardiff et al. 2013a). Correlations are strongest, in most cases, within the $10\,m \times 10\,m$ region surrounding well A1, where the majority of OHT observations were located. As well profiles or model grid cells are included far from the central observational region, the correlation between these two datasets decreases.

Second, in most cases, the use of a top model boundary condition that reflects storage changes associated with water table movement produces better results than those that assume all storage is related to compressibility (S_s). We find this result to be somewhat surprising, given that the pressure changes associated with OHT are very minor, and thus changes to the water table elevation were expected to be minimal during testing. The fact that our correlations show improvement when a more realistic water table condition is implemented suggests that observations are indeed sensitive to these near-water-table physics in unconfined aquifers.

Third, it is interesting to note that our correlation results are also substantially improved in most cases by assuming in the inversion *more* data error than would be expected from sensor instrumentation precision alone. While this is perhaps not surprising to those with experience in hydrogeophysics and inversion, it reinforces the important point that data errors used in inversion routines should represent *both* sensor error and additional errors associated with modeling approximations and other factors. This result also reinforces the understanding—well appreciated within the broader geophysical community—that "overfitting" of data (by assuming very low or no noise) can be highly detrimental to imaging efforts, especially when being applied to real-world datasets where noise, error, and conceptual modeling uncertainty are unavoidable.

Discussion

This study represents the first published field application of truly "tomographic" oscillatory hydraulic testing. Our experiments were performed at a well-characterized existing field research site where other characterization methods have been employed and assessed. Our results thus present a unique opportunity to assess the current state of OHT against more common characterization methods, and to suggest future avenues for research and improvement that could benefit future studies.

In terms of field "lessons learned," the current study used a piston setup that was capable of producing signals with a range of short periods and cycling volumes. However, the equipment used in these experiments relied on an analog speed setting for the motor that controlled piston speed and thus the actual period of the pumping signal had to be inferred from pumping well pressure records. An additional limitation of this equipment was that the flow rate signal at the pumping interval could not be directly recorded with the current setup. As summarized in Cardiff and Barrash (2015), there are many other technologies for implementing oscillatory pumping tests including oscillating solid slugs, computer-controlled pumping, pneumatic systems (McElwee et al. 2011; Sayler et al. 2018) or variation in net pumping rates at existing wells. In particular, automated methods such as computer-driven injection / extraction from a surface tank, or the use of pneumatic air injection / extraction may provide more robust methods for obtaining better control of pumping periods. In future tests in fractured rock aquifers, we plan to implement computerized pneumatic sinusoidal signals using a custom-built apparatus (similar to that employed by Sayler et al. 2018), and part of the goal of this research will be to assess the relative field performance of this method. In particular, we hope it is a more effective method for reliably controlling the amplitude and phase of head changes in the pumping well. In general, developing reliable methods for performing OHT tests will be crucial for its future application in field environments.

In comparing OHT results against prior characterization results from the BHRS, it is clear that overall correlation between HT and OHT results is strong near the centrally located B-wells, though this correlation weakens somewhat with distance from the center of the investigated volume and near the water table. In particular, areas with below-average hydraulic conductivity appear as drastically lower-K regions in the obtained OHT profiles (Figure 7). Though not shown, similar trends were observed across all analysis cases described in Table 4, and in other cases (not shown) where different near-water table storage coefficients were used. One possible reason for this discrepancy is that oscillatory tests with short periods may be more sensitive to lower-K heterogeneities (which would require more time to respond to hydraulic stimulations). In this case, we expect that the bias in HT results (which use much longer term stimulations) would be toward higher K values. However, the fact that the K values obtained by OHT are even lower than those obtained via slug tests would appear to contradict this hypothesis. Another possible reason is that even in models used that represent unconfined conditions, the model is not accurately capturing the behavior of oscillatory flows of water near the vadose zone. Indeed, it would appear to be an open question whether existing models (saturated or Richards-based) can correctly represent high-frequency oscillations of <1 min near the vadose zone, where storage effects are likely to be highly transient. Laboratory experimentation in unsaturated sandbox conditions may represent one way to assess this issue in the future.

Finally, while this study represents an initial "proof of concept" of OHT at field scales, it is by no means as comprehensive as other existing HT studies where more dense arrays of pumping and monitoring locations were implemented (e.g., Berg and Illman 2013; Berg and Illman 2014; Cardiff et al. 2012, 2013a; Hochstetler et al. 2016). Because of time limitations in the field, only a small subset of depth intervals were used for OHT-based pumping. In future work comparing OHT against other existing technologies, implementing a broader array of pumping tests and monitoring with more closely-spaced sensor intervals would doubtlessly improve resolution of subsurface features.

Acknowledgments

Test design and field experimentation were supported by NSF Awards 1215746 and 1215768. Development of the oscillating signal generator used in field experiments for this study was supported by ARO URISP award W911NF1110291 and by cost share with Mt. Sopris Instruments including design input (especially from James Koerlin). David Hochstetler and Tania Bakhos provided field assistance during collection of data.

Authors' Note

The author(s) does not have any conflicts of interest.

Supporting Information

Additional supporting information may be found online in the Supporting Information section at the end of the article. Supporting Information is generally *not* peer reviewed.

Table S1. Table containing manual test analysis information.

Table S2. Tables of site instrumentation relative positions.

Appendix. Digital Files S3: Code and datasets used to produce all manuscript analyses and figures.

References

Bakhos, T., M. Cardiff, W. Barrash, and P.K. Kitanidis. 2014. Data processing for oscillatory pumping tests. *Journal of Hydrology* 511: 310–319.

Barrash, W., and M. Cardiff. 2013. Hydraulic conductivity distribution from multi-level slug tests and multivariate

facies associations in a conglomeratic fluvial aquifer, Boise Hydrogeophysical Research Site, BSU CGISS Technical Report 13-03. https://d25vtythmttl3o.cloudfront.net/uploads/sites/290/2019/08/Barrash-and-Cardiff-K-fr-slugs-at-BHRS-CGISS-Tech-Rept-13-033.pdf (accessed August 2013).

Barrash, W., T. Clemo, J.J. Fox, and T. Johnson. 2006. Field, laboratory, and modeling investigation of the skin effect at wells with slotted casing, Boise Hydrogeophysical Research Site. *Journal of Hydrology* 326: 181–198.

Barrash, W., and E.C. Reboulet. 2004. Significance of porosity for stratigraphy and textural composition in subsurface, coarse fluvial deposits: Boise Hydrogeophysical Research Site. *Geological Society of America Bulletin* 116, no. 9/10: 1059–1073.

Barrash, W., and T. Clemo. 2002. Hierarchical geostatistics and multifacies systems: Boise Hydrogeophysical Research Site, Boise, Idaho. *Water Resources Research* 38, no 10: 1196.

Berg, S.J., and W.A. Illman. 2014. Comparison of hydraulic tomography with traditional methods at a highly heterogeneous site. *Groundwater* 53: 71–89.

Berg, S.J., and W.A. Illman. 2013. Field study of subsurface heterogeneity with steady-state hydraulic tomography. *Ground Water* 51, no. 1: 29–40.

Cardiff, M., and W. Barrash. 2015. Analytical and semi-analytical tools for the design of oscillatory pumping tests. *Groundwater* 53, no. 6: 896–907.

Cardiff, M., W. Barrash, and P.K. Kitanidis. 2013a. Hydraulic conductivity imaging from 3-D transient hydraulic tomography at several pumping/observation densities. *Water Resources Research* 49, no. 11: 7311–7326.

Cardiff, M., T. Bakhos, P.K. Kitanidis, and W. Barrash. 2013b. Aquifer heterogeneity characterization with oscillatory pumping: Sensitivity analysis and imaging potential. *Water Resources Research* 49, no. 9: 5395–5410.

Cardiff, M., W. Barrash, and P.K. Kitanidis. 2012. A field proof-of-concept of aquifer imaging using 3D transient hydraulic tomography with temporarily-emplaced equipment. *Water Resources Research* 48: W05531.

Cardiff, M., W. Barrash, B. Malama, and M. Thoma. 2011. Information content of slug tests for estimating hydraulic properties in realistic, high-conductivity aquifer scenarios. *Journal of Hydrology* 403, no. 1–2: 66–82.

Cardiff, M., W. Barrash, P.K. Kitanidis, B. Malama, A. Revil, S. Straface, and E. Rizzo. 2009. A potential-based inversion of unconfined steady-state hydraulic tomography. *Ground Water* 47, no. 2: 259–270.

Fischer, P., A. Jardani, H. Jourde, M. Cardiff, X. Wang, S. Chedeville, and N. Lecoq. 2018. Harmonic pumping tomography applied to image the hydraulic properties and interpret the connectivity of a karstic and fractured aquifer (Lez aquifer, France). *Advances in Water Resources* 119: 227–244.

Gottlieb, J., and P. Dietrich. 1995. Identification of the permeability distribution in soil by hydraulic tomography. *Inverse Problems* 11: 353–360.

Hochstetler, D.L., W. Barrash, C. Leven, M. Cardiff, F. Chidichimo, and P.K. Kitanidis. 2016. Hydraulic tomography: Continuity and discontinuity of high-K and low-K zones. *Groundwater* 54, no. 2: 171–185.

Kitanidis, P.K. 1995. Quasi-linear geostatistical theory for inversing. *Water Resources Research* 31, no. 10: 2411–2419.

Lavenue, M., and G. de Marsily. 2001. Three-dimensional interference test interpretation in a fractured aquifer using the pilot point inverse method. *Water Resources Research* 37, no. 11: 2659–2675.

McElwee, C. D., B. R. Engard, B. J. Wachter, S. A. Lyle, J. Healey, and J. F. Devlin. 2011. Hydraulic tomography and high-resolution slug testing to determine hydraulic conductivity distributions, KGS Open-File Reports (2011-02), 168.

Rabinovich, A., W. Barrash, M. Cardiff, D.L. Hochstetler, T. Bakhos, G. Dagan, and P.K. Kitanidis. 2015. Frequency dependent hydraulic properties estimated from oscillatory pumping tests in an unconfined aquifer. *Journal of Hydrology* 531: 2–16.

Renner, J., and M. Messar. 2006. Periodic pumping tests. *Geophysical Journal International* 167: 479–493.

Sayler, C., M. Cardiff, and M.D. Fort. 2018. Understanding the geometry of connected fracture flow through multi-period oscillatory hydraulic testing. *Ground Water* 56, no. 2: 276–287.

Tiedeman, C.R., and W. Barrash. 2019. Hydraulic tomography: 3D hydraulic conductivity, fracture network, and connectivity in mudstone. *Groundwater*, https://doi.org/10.1111/gwat.12915.

Zhou, Y., and M. Cardiff. 2017. Oscillatory hydraulic testing as a strategy for NAPL source zone monitoring: Laboratory experiments. *Journal of Contaminant Hydrology* 200: 24–34.

Zhou, Y., D. Lim, F. Cupola, and M. Cardiff. 2016. Aquifer imaging with pressure waves - evaluation of low-impact characterization through a sandbox study. *Water Resources Research* 52: 2141–2156.